Inorganic Chemistry
Article
pubs.acs.org/IC

Syntheses, Structures, Physical Properties, and Electronic Structures of Ba_2MLnTe_5 (M = Ga and Ln = Sm, Gd, Dy, Er, Y; M = In and Ln = Ce, Nd, Sm, Gd, Dy, Er, Y)

Wenlong Yin,[†,‡,§] Wendong Wang,[¶] Lei Bai,[†,‡] Kai Feng,[†,‡,§] Youguo Shi,[⊥] Wenyu Hao,[†,‡,§] Jiyong Yao,*[,†,‡] and Yicheng Wu[†,‡]

[†]Center for Crystal Research and Development and [‡]Key Laboratory of Functional Crystals and Laser Technology, Technical Institute of Physics and Chemistry, and [⊥]Beijing National Laboratory for Condensed Matter Physics, Institute of Physics, Chinese Academy of Sciences, Beijing 100190, China

[§]Graduate University of the Chinese Academy of Sciences, Beijing 100049, China

[¶]School of Science, Beijing University of Post and Telecommunication, Beijing 100876, China

Supporting Information

ABSTRACT: The 12 new rare-earth tellurides Ba_2MLnTe_5 (M = Ga and Ln = Sm, Gd, Dy, Er, Y; M = In and Ln = Ce, Nd, Sm, Gd, Dy, Er, Y) have been synthesized by solid-state reactions. The two compounds $Ba_2GaLnTe_5$ (Ln = Sm, Gd) are isostructural and crystallize in the centrosymmetric space group $P\bar{1}$, while the other 10 compounds belong to another structure type in the noncentrosymmetric space group $Cmc2_1$. In both structure types, there are one-dimensional anionic ${}^{\infty}_{1}[MLnTe_5]^{4-}$ chains built from $LnTe_6$ octahedra and MTe_4 (M = Ga, In) tetrahedra, but the connectivity between the $LnTe_6$ octahedra and MTe_4 tetrahedra is different for the two structure types. On the basis of the diffuse-reflectance spectra, the band gaps are around 1.1−1.3 eV for these compounds. The Ba_2MLnTe_5 (M = Ga and Ln = Gd, Dy; M = In and Ln = Gd, Dy, Er) compounds are paramagnetic and obey the Curie−Weiss law, while the magnetic susceptibility of $Ba_2InSmTe_5$ deviates from the Curie−Weiss law. In addition, electronic structure calculation on Ba_2MYTe_5 (M = Ga, In) indicates that they are both direct-gap semiconductors with large nonlinear-optical coefficients.

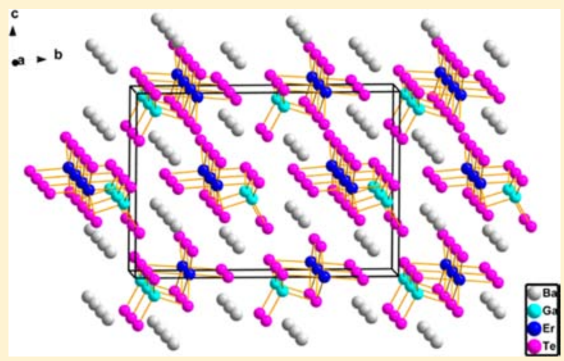

■ INTRODUCTION

Extensive efforts in the synthesis and characterization of rare-earth chalcogenides have led to the discovery of many new multinary rare-earth chalcogenides with intriguing structures and interesting magnetic, electronic, luminescent, thermoelectric, and nonlinear-optical (NLO) properties.[1−30] One subset of rare-earth chalcogenides that have received increasing attention are those containing the combination of a rare-earth metal and a main-group p-block element. For example, $ZnY_6Si_2S_{14}$,[9] $La_2Ga_2GeS_8$,[10] $Eu_2Ga_2GeS_7$,[10] La_4InSbS_9,[11] Sm_4GaSbS_9,[12] and Ba_2InYSe_5[30] compounds, especially the latter four, were reported to exhibit strong second-harmonic-generation (SHG) responses in the middle IR. Recently, we carried out a systematic investigation of the quaternary A/M/Ln/Q (A = alkaline-earth metal; M = group IIIA metal Ga and In; Ln = rare-earth metal; Q = chalcogen) system in the hope of discovering new multifunctional materials through the combination of magnetic rare-earth cations and MQ_4 units (M = Ga, In; Q = chalcogen), which are the typical functional groups in NLO chalcogenides, and through the interplay of covalent M−Q bonding with ionic Ln−Q or A−Q bonding. In an earlier study, we reported the synthesis and characterization of 12 new selenides in this family, namely, the Ba_2MLnSe_5 (M = Ga, In; Ln = Y, Nd, Sm, Gd, Dy, Er) compounds,[30] which exhibit two different structure types. Besides, $Ba_2GaGdSe_5$ and $Ba_2InLnSe_5$ (Ln = Nd, Gd, Dy, Er) are paramagnetic and obey the Curie−Weiss law, and Ba_2InYSe_5 exhibits a strong SHG response close to that of $AgGaSe_2$.

So far, most of these chalcogenides containing both an f-block rare-earth metal and a p-block main-group element are sulfides and selenides, and many fewer tellurides are reported. Because of the more diffuse nature of the 5p orbitals, the smaller electronegativity, and the larger radius of the Te atom, tellurides often exhibit different structures and properties from sulfides and selenides. For example, the $CsLnZnTe_3$ tellurides could be synthesized over the entire range of Ln elements, while the corresponding $CsLnZnSe_3$ selenides could not be synthesized for Ln elements larger than Sm, which demonstrated that the larger tetrahedral and octahedral sites in the Te layers are more accommodating compared with those in the Se layers.[20,21] More interestingly, tellurium can exhibit a wide

Received: July 27, 2012
Published: October 9, 2012

Table 1. Crystal Data and Structure Refinements for $Ba_2GaLnTe_5$ (Ln = Sm, Gd, Dy, Er, Y)

	$Ba_2GaSmTe_5$	$Ba_2GaGdTe_5$	$Ba_2GaDyTe_5$	$Ba_2GaErTe_5$	Ba_2GaYTe_5
fw	1132.75	1139.65	1144.90	1149.66	1071.31
T (K)	293(2)	293(2)	293(2)	153(2)	153(2)
a (Å)	7.7785(3)	7.7759(7)	4.4638(1)	4.4404(9)	4.4412(9)
b (Å)	9.2641(4)	9.2361(6)	20.0925(5)	20.001(4)	20.035(4)
c (Å)	10.0750(3)	10.0635(8)	14.0899(3)	14.034(3)	14.053(3)
α (deg)	103.399(3)	103.347(6)	90.00	90.00	90.00
β (deg)	102.894(3)	102.887(8)	90.00	90.00	90.00
γ (deg)	107.429(4)	107.406(5)	90.00	90.00	90.00
V (Å^3)	639.47(4)	636.96(9)	1263.71(5)	1246.5(4)	1250.4(4)
space group	$P\bar{1}$	$P\bar{1}$	$Cmc2_1$	$Cmc2_1$	$Cmc2_1$
Z	2	2	4	4	4
ρ_c (g/cm^3)	5.883	5.942	6.018	6.126	5.691
μ (mm^{-1})	23.801	24.491	25.354	26.443	24.312
$R(F)^a$	0.0352	0.0379	0.0328	0.0266	0.0350
$R_w(F_o^2)^b$	0.0966	0.0875	0.0591	0.0635	0.0890

$^aR(F) = \sum||F_o| - |F_c||/\sum|F_o|$ for $F_o^2 > 2\sigma(F_o^2)$. $^bR_w(F_o^2) = \{\sum[w(F_o^2 - F_c^2)^2]/\sum wF_o^4\}^{1/2}$ for all data. $w^{-1} = \sigma^2(F_o^2) + (z\,P)^2$, where $P = (\max(F_o^2, 0) + 2F_c^2)/3$.

range of interactions intermediate to the Te–Te single-bond length and the van der Waals interaction of about 4.1 Å. The presence of such intermediate distances in tellurides such as $Cs_5Hf_5Te_{26}$ [Te⋯Te distances ranging from 2.741(8) to 3.474(9) Å] renders the assignment of formal charges impossible.[31] This propensity of Te profoundly affects the structural chemistry and physical properties of tellurides. For example, $LnTe_3$ exhibits valence fluctuations with the unusual formal valence representations $(LnTe)^+(Te_2)^-$ and shows two-dimensional charge-density wave behavior.[32]

As for IR NLO materials, most of the newly found IR NLO materials are also sulfides and selenides and few are tellurides. From the current understanding of the composition–structure–property relationship of NLO chalcogenide compounds, as the chalcogen element goes from S to Se and then to Te, the SHG effect of the compounds will increase considerably and the IR absorption edge will red-shift significantly. For example, the NLO coefficient increases from 13.4 pm/V for $AgGaS_2$ to 33 pm/V for $AgGaSe_2$ and to 76.6 pm/V for $AgGaTe_2$, and the IR absorption edge red-shifts from 13 μm for $AgGaS_2$ to 18 μm for $AgGaSe_2$ and to 21 μm for $AgGaTe_2$.[33−36] A larger NLO coefficient will increase the laser conversion efficiency and longer IR absorption will make the materials suitable for application in the far-IR or even the terahertz range. Actually, the search for NLO materials in the far-IR and terahertz ranges may represent a major direction in future NLO materials research. In this respect, the current materials, such as $AgGaTe_2$, suffer from a low laser-damage threshold.

Thus, it is worthwhile to expand our exploration to tellurides owing to their unique structural features and promising properties. In this paper, we detail the synthesis, structural characterization, and physical properties of 12 new tellurides, namely, the Ba_2MLnTe_5 (M = Ga and Ln = Sm, Gd, Dy, Er, Y; M = In and Ln = Ce, Nd, Sm, Gd, Dy, Er, Y) compounds. In addition, we calculate the electronic structures and NLO coefficients of Ba_2MYTe_5 (M = Ga, In).

■ EXPERIMENTAL SECTION

Syntheses. The following reagents were used as obtained: Ba (Aladdin Co., Ltd., 99%), Ga (Sinopharm Chemical Reagent Co., Ltd., 99.99%), In (Sinopharm Chemical Reagent Co., Ltd., 99.99%), Te (Sinopharm Chemical Reagent Co., Ltd., 99.99%), and Ln [Ln = Ce, Nd, Sm, Gd, Dy, Er, Y; Alfa Aesar China (Tianjin) Co., Ltd., 99.9%]. The binary starting materials BaTe, Ga_2Te_3, and In_2Te_3 were prepared by the stoichiometric reactions of the elements at high temperatures in sealed silica tubes evacuated to 10^{-3} Pa.

$Ba_2GaLnTe_5$ (Ln = Sm, Gd, Dy, Er, Y). Reaction mixtures of 1 mmol of BaTe, 0.25 mmol of Ga_2Te_3, 0.5 mmol of Ln, and 0.75 mmol of Te were loaded into fused-silica tubes under an Ar atmosphere in a glovebox. These tubes were sealed under a 10^{-3} Pa atmosphere, then placed in computer-controlled furnaces, heated to 1323 K in 24 h, left for 48 h, cooled to 593 K at a rate of 3 K/h, and finally cooled to room temperature by switching off the furnace. Block-shaped crystals with the color of black were found in the ampules. The crystals are stable in air.

$Ba_2InLnTe_5$ (Ln = Ce, Nd, Sm, Gd, Dy, Er, Y). Reaction mixtures of 1 mmol of BaTe, 0.25 mmol of In_2Te_3, 0.5 mmol of Ln, and 0.75 mmol of Te were ground, loaded into fused-silica tubes under an Ar atmosphere in a glovebox, and then flame-sealed under a high vacuum of 10^{-3} Pa. The tubes were then placed in computer-controlled furnaces, heated to 1273 K in 20 h, left for 48 h, cooled to 593 K at a rate of 2 K/h, and finally cooled to room temperature by switching off the furnace. Black block-shaped crystals were found in the ampules. The crystals are stable in air.

The crystals were manually selected for structural characterization and were later determined as Ba_2MLnTe_5 (M = Ga and Ln = Sm, Gd, Dy, Er, Y; M = In and Ln = Ce, Nd, Sm, Gd, Dy, Er, Y). Analyses of the crystals with an energy-dispersive X-ray (EDX)-equipped Hitachi S-4800 scanning electron microscope proved the presence of Ba, M (M = Ga, In), Ln, and Te in the approximate ratio of 2:1:1:5.

Polycrystalline samples were synthesized by solid-state reaction techniques. The mixtures of BaTe, In_2Te_3, and Te in a molar ratio of 4:1:2:3 were heated to 1173 K in 20 h and kept at that temperature for 72 h, and then the furnace was turned off. The experimental powder X-ray diffraction patterns were in agreement with the calculated patterns on the basis of the single-crystal crystallographic data, and the results are presented in the Supporting Information, Figure S1.

Structural Determination. The single-crystal X-ray diffraction measurements were performed on a Rigaku AFC10 diffractometer equipped with graphite-monochromated Kα (λ = 0.71073 Å) radiation. The *Crystalclear* software[37] was used for data extraction and integration, and the program *XPREP*[38] was used for face-indexed absorption corrections.

The structure was solved with direct methods implemented in the program *SHELXS* and refined with the least-squares program *SHELXL* of the *SHELXTL.PC* suite of programs.[38] The program *STRUCTURE TIDY*[39] was then employed to standardize the atomic coordinates. Additional experimental details are given in Tables 1 and 2, and

Table 2. Crystal Data and Structure Refinements for $Ba_2InLnTe_5$ (Ln = Ce, Nd, Sm, Gd, Dy, Er, Y)[a]

	$Ba_2InCeTe_5$	$Ba_2InNdTe_5$	$Ba_2InSmTe_5$	$Ba_2InGdTe_5$	$Ba_2InDyTe_5$	$Ba_2InErTe_5$	Ba_2InYTe_5
fw	1167.62	1171.74	1177.85	1184.75	1190.00	1194.76	1116.41
a (Å)	4.5781(9)	4.5579(9)	4.5349(9)	4.5014(9)	4.5198(9)	4.4998(9)	4.5137(9)
b (Å)	20.292(4)	20.194(4)	20.151(4)	20.064(4)	20.065(4)	20.070(4)	20.087(4)
c (Å)	14.079(3)	14.104(3)	14.086(3)	14.078(3)	14.089(3)	14.079(3)	14.093(3)
V (Å^3)	1308.0(5)	1298.1(4)	1287.3(4)	1271.5(4)	1277.7(4)	1271.5(4)	1277.7(4)
Flack parameter	0.03(5)	−0.01(4)	−0.02(3)	−0.09(3)	0.04(2)	−0.02(2)	−0.01(2)
ρ_c (g/cm^3)	5.929	5.995	6.078	6.189	6.186	6.241	5.804
μ (mm^{-1})	21.967	22.626	23.345	24.234	24.772	25.617	23.488
$R(F)^b$	0.0351	0.0356	0.0302	0.0318	0.0298	0.0275	0.0311
$R_w(F_o^2)^c$	0.0629	0.0687	0.0624	0.0698	0.0601	0.0541	0.0581

[a]For all structures, $Z = 4$, space group = $Cmc2_1$, $T = 153$ (2) K, and $\lambda = 0.71073$ Å. [b]$R(F) = \sum||F_o| - |F_c||/\sum|F_o|$ for $F_o^2 > 2\sigma(F_o^2)$. [c]$R_w(F_o^2) = \{\sum[w(F_o^2 - F_c^2)^2]/\sum wF_o^4\}^{1/2}$ for all data. $w^{-1} = \sigma^2(F_o^2) + (zP)^2$, where $P = (\max(F_o^2, 0) + 2F_c^2)/3$.

Table 3. Selected Interatomic Distances (Å) for $Ba_2GaLnTe_5$ (Ln = Sm, Gd, Dy, Er, Y)

	$Ba_2GaSmTe_5$	$Ba_2GaGdTe_5$		$Ba_2GaDyTe_5$	$Ba_2GaErTe_5$	Ba_2GaYTe_5
Ga−Te1	2.556(1)	2.563(2)	Ga−Te4	2.570(1)	2.567(2)	2.563(2)
Ga−Te3	2.620(1)	2.614(2)	Ga−Te3	2.697(1)	2.692(2)	2.700(2)
Ga−Te2	2.622(1)	2.615(2)	Ga−Te5	2.7187(7)	2.706(1)	2.706(1)
Ga−Te5	2.721 (1)	2.718(2)	Ga−Te5	2.7187(7)	2.706(1)	2.706(1)
Ln−Te4	3.0731(7)	3.052(1)	Ln−Te1	2.9815(6)	2.956(1)	2.972(2)
Ln−Te4	3.0740(8)	3.053(1)	Ln−Te2	3.0260(4)	3.0024(8)	3.014(1)
Ln−Te3	3.1213(8)	3.106(1)	Ln−Te2	3.0260(4)	3.0023(8)	3.014(1)
Ln−Te2	3.1251(8)	3.110(1)	Ln−Te3	3.1349(5)	3.1098(9)	3.123(1)
Ln−Te5	3.2213(8)	3.215(1)	Ln−Te3	3.1349(5)	3.1098(9)	3.123(1)
Ln−Te5	3.2215(7)	3.217(1)	Ln−Te5	3.2207(7)	3.195(1)	3.212(2)

Table 4. Selected Interatomic Distances (Å) for $Ba_2InLnTe_5$ (Ln = Ce, Nd, Sm, Gd, Dy, Er, Y)

	$Ba_2InCeTe_5$	$Ba_2InNdTe_5$	$Ba_2InSmTe_5$	$Ba_2InGdTe_5$	$Ba_2InDyTe_5$	$Ba_2InErTe_5$	Ba_2InYTe_5
In−Te4	2.720(2)	2.717(2)	2.714(1)	2.709(2)	2.708(2)	2.706(2)	2.708(2)
In−Te5×2	2.8187(8)	2.8133(9)	2.8042(8)	2.794(1)	2.8034(9)	2.7931(9)	2.7977(9)
In−Te3	2.876(2)	2.873(2)	2.876(2)	2.863(2)	2.867(2)	2.870(2)	2.870(2)
Ln−Te1	3.073(2)	3.045(1)	3.021(1)	2.961(1)	2.974(1)	2.962(1)	2.978(2)
Ln−Te2×2	3.1180(9)	3.096(1)	3.0685(8)	3.020(1)	3.0343(8)	3.0157(9)	3.032(1)
Ln−Te3×2	3.230(1)	3.207(1)	3.1822(9)	3.127(1)	3.1501(9)	3.1282(9)	3.146(1)
Ln−Te5	3.349(2)	3.310(2)	3.285(1)	3.231(2)	3.245(1)	3.233(1)	3.246(2)

selected metrical data are given in Tables 3 and 4. Further information may be found in the Supporting Information.

Diffuse-Reflectance Spectroscopy. A Cary 1E UV−visible spectrophotometer with a diffuse-reflectance accessory was used to measure the spectra of Ba_2MLnTe_5 (M = Ga and Ln = Sm, Gd, Dy, Er, Y; M = In and Ln = Ce, Nd, Sm, Gd, Dy, Er, Y) over the range 300 nm (4.13 eV) to 2150 nm (0.58 eV).

Magnetic Susceptibility Measurements. Single crystals of Ba_2MLnTe_5 (M = Ga and Ln = Gd, Dy; M = In and Ln = Sm, Gd, Dy, Er) (about 10 mg) were ground and loaded into gelatin capsules for the measurement of magnetism. The magnetic susceptibilities were measured by using a Quantum Design SQUID magnetometer (MPMS7T Quantum Design) between 2 and 300 K in an applied field of 10 kOe. The samples were gathered in a sample holder and cooled to the low-temperature limit. The magnetic field was then applied to the samples, and then the samples were slowly warmed to 300 K (zero-field cooling, ZFC), followed by cooling in the field (field cooling, FC). The susceptibility was calculated by dividing by the applied field.

SHG Measurement. Optical SHG tests of Ba_2MLnTe_5 (M = Ga and Ln = Dy, Er, Y; M = In and Ln = Ce, Nd, Sm, Gd, Dy, Er, Y) were performed by means of the Kurtz−Perry method.[40] Fundamental 2090 nm light was generated with a Q-switched Ho:Tm:Cr:YAG laser. The particle sizes of the sieved samples are 80−100 μm. Microcrystalline $AgGaSe_2$ of similar particle size served as a reference.

Theoretical Calculation. The electronic properties were calculated using the plane-wave pseudopotential method,[41] implemented in the CASTEP package.[42] Local density approximations (LDAs) with high kinetic-energy cutoffs of 800 and 400 eV were adopted for Ba_2GaYTe_5 and Ba_2InYTe_5 calculations, respectively. The preconditioned conjugated-gradient band-by-band method[43] used in CASTEP ensures a robust efficient search of the energy minimum of the electronic structure ground state. The optimized normal-conserving pseudopotentials[44] in Kleinman−Bylander form[45] for Ba, Ga, In, Y, and Te allow us to use a small plane-wave basis set without compromising the accuracy required by our study. The electron orbitals 5s, 5p, 5d, and 6s for Ba are chosen as the valence electrons. For Ga, they are 3d, 4s, and 4p. For In and Te, they are 5s and 5p. At last, for Y, 4d and 5s are chosen as the valence electrons. Monkhorst−Pack k-point meshes[46] with a density of 3 × 1 × 1 points in the Brillouin zone of their unit cell were chosen.

■ RESULTS AND DISCUSSION

Synthesis. A total of 12 new tellurides Ba_2MLnTe_5 (M = Ga and Ln = Sm, Gd, Dy, Er, Y; M = In and Ln = Ce, Nd, Sm, Gd, Dy, Er, Y) have been synthesized by traditional high-temperature solid-state reactions. The yields of crystals varied from 10% to 40% based on Ln, and the remaining products were mainly the powders of Ba_2MLnTe_5 based on X-ray diffraction analysis. Considering the high reaction temperatures and the easy formation of these Ba_2MLnTe_5 compounds, they are probably thermodynamically stable compounds. We also tried to synthesize analogues containing other rare-earth elements available to us, namely, La, Pr, Tb, Ho, and Yb, but failed. We have also explored the sulfides in this system. Surprisingly, the sulfides possess totally different stoichiometries and structures from the selenides and tellurides, which clearly demonstrates the richness of the phases in this system. Owing to their different stoichiometries and structures, the sulfides will be reported separately.

Structure. *$Ba_2GaLnTe_5$ (Ln = Sm, Gd).* The two Ga-containing compounds $Ba_2GaLnTe_5$ (Ln = Sm, Gd) are isostructural. They belong to the Ba_2GaYSe_5 structure type[30] and crystallize in the centrosymmetric space group $P\bar{1}$ of the triclinic system. In the asymmetric unit, there are two crystallographically independent Ba atoms, one independent Ga atom, one Ln atom, and five Te atoms, all at general positions with 100% occupancy. The Ba atoms are coordinated to a bicapped trigonal prism of eight Te atoms. The Ln atoms are coordinated to a slightly distorted octahedron of six Te atoms, whereas the Ga atoms are coordinated to a distorted tetrahedron of four Te atoms. The shortest Te···Te distance of 4.022(2) Å in the two compounds indicates that there is no bonding interaction between the Te atoms. Thus, the oxidation states of 2+, 3+, 3+, and 2− can be assigned to Ba, Ga, Ln, and Te, respectively.

The structure of $Ba_2GaSmTe_5$ is illustrated in Figure 1. The structure features infinite one-dimensional $^{\infty}_{1}[GaSmTe_5]^{4-}$ anionic chains built from $SmTe_6$ octahedra and $GaTe_4$ tetrahedra. The $SmTe_6$ octahedra are connected to each other by edge-sharing to form a chain, and then the isolated $GaTe_4$ tetrahedra are attached on the two sides of the chain of $SmTe_6$ octahedra via edge-sharing to produce the infinite one-dimensional $^{\infty}_{1}[GaSmTe_5]^{4-}$ anionic chains (Figure 2), which are parallel along the *b*-axis direction and separated by Ba^{2+} cations.

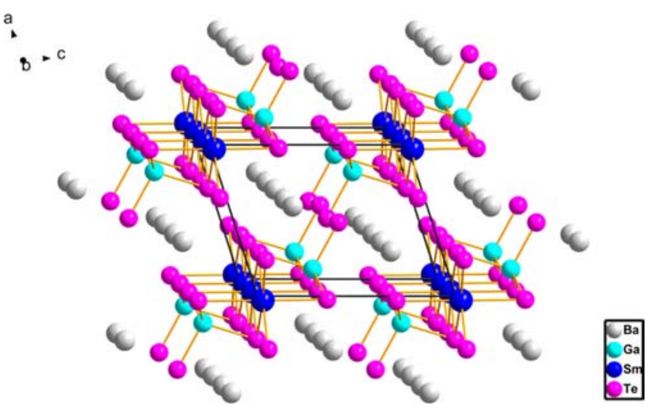

Figure 1. Unit cell of the $Ba_2GaSmTe_5$ structure.

$Ba_2GaLnTe_5$ (Ln = Dy, Er, Y) and $Ba_2InLnTe_5$ (Ln = Ce, Nd, Sm, Gd, Dy, Er, Y). The other three Ga-containing compounds $Ba_2GaLnTe_5$ (Ln = Dy, Er, Y) and the seven In-containing compounds $Ba_2InLnTe_5$ (Ln = Ce, Nd, Sm, Gd, Dy, Er, Y) are isostructural. They belong to the Ba_2BiInS_5 structure type[47] and crystallize in the noncentrosymmetric space group $Cmc2_1$ of the orthorhombic system. The asymmetric unit contains two crystallographically unique Ba atoms, one M (M = Ga, In) atom, one Ln atom, and five Te atoms, all at the Wyckoff positions 4a with m symmetry. For all these 10 compounds, each Ba1 atom is coordinated to seven Te atoms in a monocapped trigonal-prismatic geometry, while each Ba2 atom is coordinated to eight Te atoms in a bicapped trigonal-prismatic geometry; each Ln atom is coordinated to six Te atoms to form a distorted octahedron, and each M (M = Ga, In) atom is coordinated to four Te atoms in a distorted tetrahedral arrangement. The shortest Te···Te distance in all these 10 compounds is 4.028(2) Å, which excludes the possibility of any, even partial, bonding interactions between the Te atoms. Hence, the oxidation states of 2+, 3+, 3+, and 2− can be assigned to Ba, M, Ln, and Te, respectively.

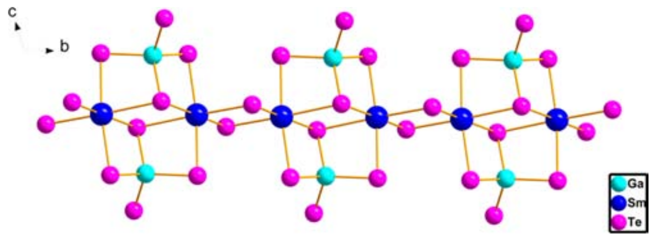

Figure 2. $^{\infty}_{1}[GaSmTe_5]^{4-}$ anionic chain in $Ba_2GaSmTe_5$.

As illustrated in Figure 3, the structure of $Ba_2GaErTe_5$ contains one-dimensional $^{\infty}_{1}[GaErTe_5]^{4-}$ anionic chains separated by charge-compensating Ba^{2+} cations. Each $ErTe_6$ octahedron shares edges with two other $ErTe_6$ octahedra to form a one-dimensional $^{\infty}_{1}[ErTe_4]^{5-}$ chain along the *a* direction. The $GaTe_4$ tetrahedra themselves generate another kind of one-dimensional $^{\infty}_{1}[GaTe_3]^{3-}$ chain along the *a* direction via corner-sharing. These two kinds of chains are further interconnected with each other through common Te atoms to generate the $^{\infty}_{1}[GaErTe_5]^{4-}$ anionic chains running along the *a* direction (Figure 4).

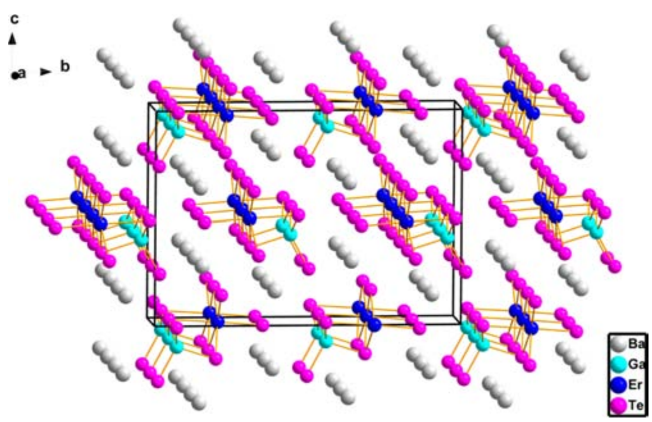

Figure 3. Unit cell of the $Ba_2GaErTe_5$ structure.

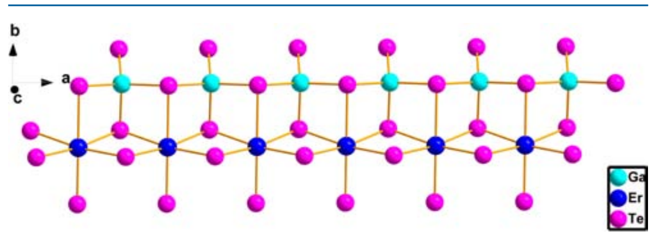

Figure 4. $^{\infty}_{1}[InErTe_5]^{4-}$ anionic chain in $Ba_2GaErTe_5$.

dx.doi.org/10.1021/ic301655e | *Inorg. Chem.* 2012, 51, 11736−11744

Selected bond distances for all 12 compounds are displayed in Tables 3 and 4, and the Ba–Te distances are presented in Tables S1 and S2 in the Supporting Information. All bond lengths are normal for a $BaTe_7$ monocapped trigonal prism, a $BaTe_8$ bicapped trigonal prism, MTe_4 (M = Ga, In) tetrahedra, and $LnTe_6$ octahedra, respectively. For example, the Ba–Te distances range from 3.404(1) to 3.947(1) Å, which resemble those of 3.538(2)–3.745(2) Å in $BaSm_2Te_4$;[48] the Ga–Te distances vary from 2.556(1) to 2.721 (1) Å and agree with those of 2.586(1)–2.676(1) Å in $YbGa_6Te_{10}$;[49] the In–Te distances of 2.706(2)–2.876(2) Å are comparable to those of 2.758(1)–2.839(1) Å in $PbIn_6Te_{10}$;[50] the Ln–Te distances, ranging from 2.962(1) to 3.349(2) Å, are consistent with the previously reported distances of 3.0296(7)–3.3585(5) Å in $CsLnZnTe_3$,[21] $CsLnCdTe_3$,[1] and $K_2Ag_3CeTe_4$.[3]

The structural difference between $Ba_2GaLnTe_5$ (Ln = Sm, Gd; space group $P\bar{1}$) and $Ba_2GaLnTe_5$ (Ln = Dy, Er, Y; space group $Cmc2_1$) results from the different connectivities between the $GaTe_4$ tetrahedra and $LnTe_6$ octahedra. In $Ba_2GaLnTe_5$ (Ln = Sm, Gd), the isolated $GaTe_4$ tetrahedra are located on both sides of the chain of $LnTe_6$ octahedra, and inversion centers can be found between the $GaTe_4$ tetrahedra, while the $GaTe_4$ tetrahedra in the other three compounds $Ba_2GaLnTe_5$ (Ln = Dy, Er, Y) share corners to form a one-dimensional chain on only one side of the chain of $LnTe_6$ octahedra.

The different packing modes of the $GaTe_4$ tetrahedra between $Ba_2GaLnTe_5$ (Ln = Sm, Gd; space group $P\bar{1}$) and $Ba_2GaLnTe_5$ (Ln = Dy, Er, Y) are probably due to the different sizes of the Ln^{3+} cations because Sm^{3+} and Gd^{3+} are bigger than Dy^{3+}, Er^{3+}, and Y^{3+}, so for the compounds $Ba_2GaLnTe_5$ (Ln = Sm, Gd), the Ga–Te bond length may be not long enough to form a one-dimensional chain, which could match the chain of $LnTe_6$ octahedra for Ln = Sm, Gd in view of the interatomic spacing, despite distortion of the $GaTe_4$ tetrahedra. In other words, the one-dimensional ${}^{\infty}_{1}[GaTe_3]^{3-}$ chain could match the one-dimensional ${}^{\infty}_{1}[LnTe_4]^{5-}$ chain only when the rare-earth cations are the smaller Dy^{3+}, Er^{3+}, and Y^{3+}. Similarly, because the In–Te bonds are longer than the Ga–Te bonds, the one-dimensional $InTe_4$ tetrahedra chain could match the chain of $LnTe_6$ octahedra for both the large and small rare-earth elements through distortion of the $InTe_4$ tetrahedra. Thus, all seven In-containing compounds $Ba_2InLnTe_5$ (Ln = Ce, Nd, Sm, Gd, Dy, Er, Y) are isostructural with the $Ba_2GaLnTe_5$ (Ln = Dy, Er, Y; space group $Cmc2_1$).

Considering the size ratio of Ln^{3+}/M^{3+} (Ln = rare earth; M = Ga, In) in these 12 tellurides, the two gallium tellurides adopting the $P\bar{1}$ structure type have the largest Ln^{3+}/M^{3+} ratios of 1.8 and 1.767. Also, for compounds with smaller Ln^{3+}/M^{3+} ratios ranging from 1.724 to 1.355, they all adopt the $Cmc2_1$ structure type. In comparison, in the 12 selenides reported earlier, Ln^{3+}/M^{3+} ratios for the six selenides adopting the $P\bar{1}$ structure type range from 1.84 for Nd^{3+}/Ga^{3+} to 1.688 for Er^{3+}/Ga^{3+}, while those for the six selenides adopting the $Cmc2_1$ structure type lie in the range of 1.477 for Nd^{3+}/In^{3+} to 1.355 for Er^{3+}/In^{3+}.[51] Clearly, the effect of the Ln^{3+}/M^{3+} ratio on the crystal structures is different for selenides and tellurides. The effect of cation sizes on the crystal structures has also been shown in many series of compounds.[52,53]

Experimental Band Gaps. On the basis of the UV–visible–near-IR diffuse-reflectance spectra of Ba_2MLnTe_5 (M = Ga and Ln = Sm, Gd, Dy, Er, Y; M = In and Ln = Ce, Nd, Sm, Gd, Dy, Er, Y; Figures 5 and 6), the band gaps can be deduced by the straightforward extrapolation method.[54] As shown in Table 5, the band gaps range from 1.04(2) to 1.15(2) eV for the Ga-containing compounds and around 1.35(2) eV for the In-containing compounds. As shown in Figures 5 and 6, all of the compounds have strong absorption in the entire measured wavelength range from 300 to 2150 nm.

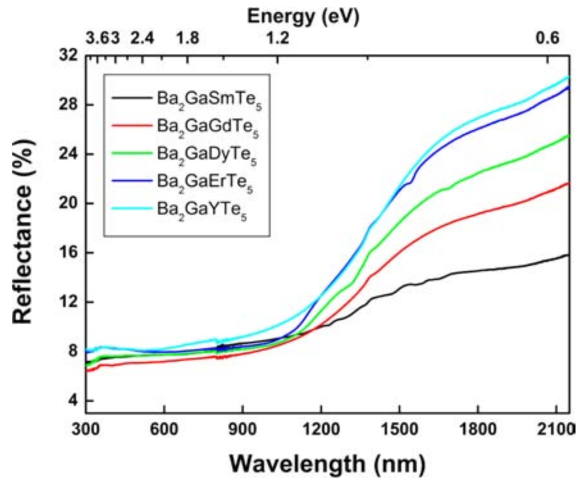

Figure 5. Diffuse-reflectance spectra of $Ba_2GaLnTe_5$ (Ln = Sm, Gd, Dy, Er, Y).

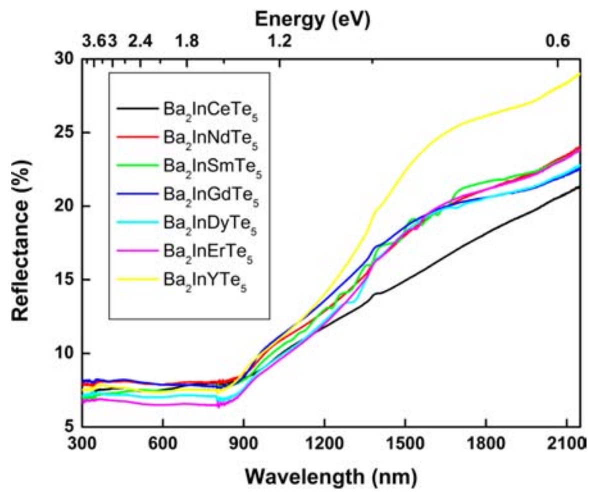

Figure 6. Diffuse-reflectance spectra of $Ba_2GaLnTe_5$ (Ln = Ce, Nd, Sm, Gd, Dy, Er, Y).

Table 5. Band Gaps of Ba_2MLnTe_5 (M = Ga and Ln = Sm, Gd, Dy, Er, Y; M = In and Ln = Ce, Nd, Sm, Gd, Dy, Er, Y)

compound	band gap (eV)	compound	band gap (eV)
		$Ba_2InCeTe_5$	1.35(2)
		$Ba_2InNdTe_5$	1.37(2)
$Ba_2GaSmTe_5$	1.04(2)	$Ba_2InSmTe_5$	1.36(2)
$Ba_2GaGdTe_5$	1.12(2)	$Ba_2InGdTe_5$	1.36(2)
$Ba_2GaDyTe_5$	1.13(2)	$Ba_2InDyTe_5$	1.35(2)
$Ba_2GaErTe_5$	1.15(2)	$Ba_2InErTe_5$	1.35(2)
Ba_2GaYTe_5	1.08(2)	Ba_2InYTe_5	1.36(2)

Such band gaps are obviously smaller than those of the $CsLnMTe_3$ (M = Zn, Cd) compounds (2.1 eV for M = Zn and 2.0 eV for M = Cd).[1,21] Clearly, the orbitals of the group IIIA elements and those of the group IIB elements have significantly different influences on the band gap because the orbitals of Cs

dx.doi.org/10.1021/ic301655e | Inorg. Chem. 2012, 51, 11736–11744

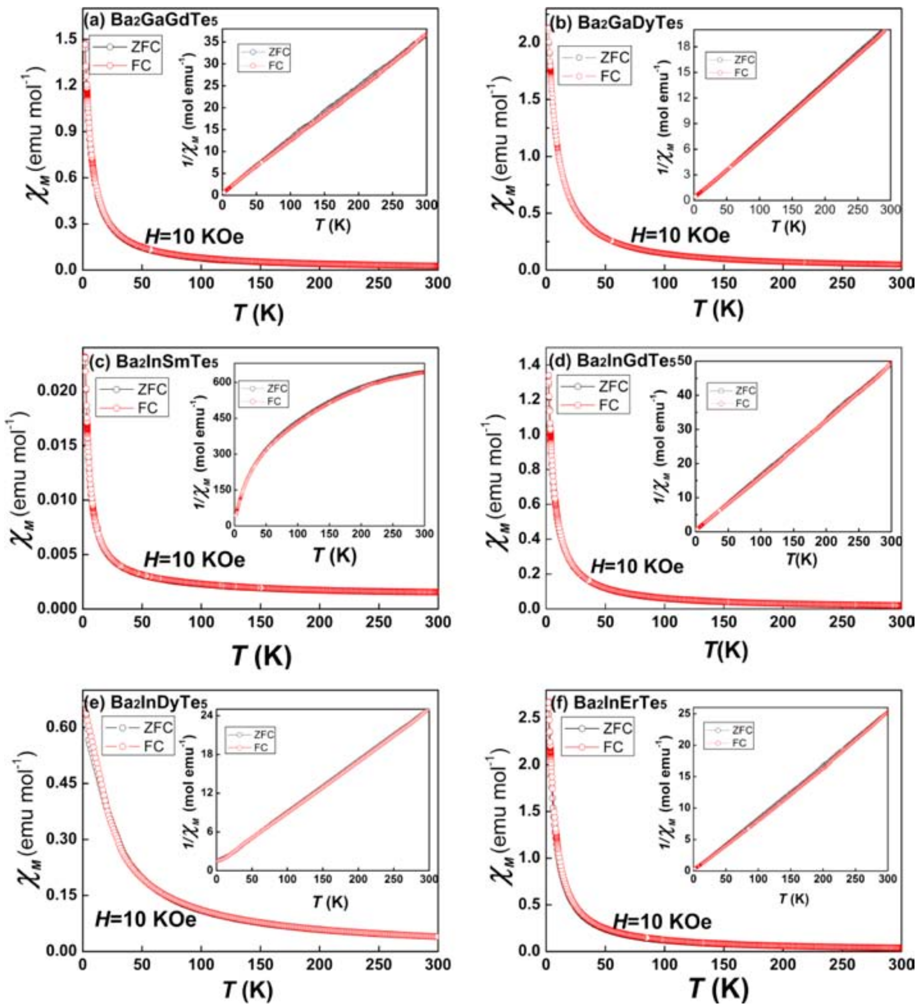

Figure 7. χ_m vs T of Ba_2MLnTe_5 (M = Ga and Ln = Gd, Dy; M = In and Ln = Sm, Gd, Dy, Er) for FC and ZFC data. Inset: plot of $1/\chi_m$ vs T.

in $CsLnMTe_3$ (M = Zn, Cd) and Ba in Ba_2MLnTe_5 (M = Ga, In) have minimal influence on the optical band gap (see the Electronic Structure Calculation section). Furthermore, the trend of the smaller band gaps for Ga-containing compounds and larger ones for In-containing compounds is not seen in the AMQ_2 (A = Li, Ag; M = Ga, In; Q = chalcogen) series of compounds,[55,56] which do not contain the rare-earth elements. As far as we know, no data could be found in the literature to compare the trend of band gaps between the Ga- and In-containing chalcogenides that have both group IIIA and rare-earth elements. The interesting band-gap trend of the Ga- and In-containing compounds in Ba_2MLnTe_5 (M = Ga, In) may be worth further study in the future.

Magnetic Susceptibility Measurements. Temperature dependence of the molar magnetic susceptibilities (χ_m) and the inverse magnetic susceptibilities ($1/\chi_m$) for Ba_2MLnTe_5 (M = Ga and Ln = Gd, Dy; M = In and Ln = Sm, Gd, Dy, Er) are shown in Figure 7. The ZFC and FC magnetic susceptibility data are essentially superimposable at all temperatures. The susceptibility data were fit by a least-squares method to the Curie−Weiss equation $\chi_m = C/(T - \theta)$, where C is the Curie constant and θ is the Weiss constant. The effective magnetic moments [μ_{eff}(total)] were calculated from the equation $\mu_{eff}(\text{total}) = (7.997C)^{1/2}\mu_B$.[57]

As shown in Figure 7, they are paramagnetic and obey the Curie−Weiss law over the entire experimental temperature range except for $Ba_2InSmTe_5$. Table 6 shows the values of C and θ generated by the linear fitting of $1/\chi_m$ with T over the whole temperature and the calculated effective magnetic moments μ_{eff} for each compound except for $Ba_2InSmTe_5$. The calculated effective magnetic moments are close to the theoretical values for the Ln^{3+} ion.[58] The negative θ values for the Gd- and Dy-containing tellurides Ba_2MLnTe_5 (M = Ga, In; Ln = Gd, Dy) may indicate weak short-range antiferromagnetic interaction among the adjacent Ln^{3+} cations, while the small positive θ value for $Ba_2InErTe_5$ may indicate rather weak short-range ferromagnetic interaction among the Er^{3+} cations. The magnetic data for $Ba_2InSmTe_5$ do not follow the Curie−Weiss law because its effective magnetic moment of the 4f electrons has a temperature dependence arising from low-lying

Table 6. Magnetic Properties of Ba_2MLnTe_5 (M = Ga and Ln = Gd, Dy; M = In and Ln = Gd, Dy, Er)

			μ_{eff} (μ_B)	
compound	C (emu·K/mol)	θ (K)	obs	theory
$Ba_2GaGdTe_5$	8.35	−7.33	8.17	7.94
$Ba_2GaDyTe_5$	14.62	−2.20	10.81	10.63
$Ba_2InGdTe_5$	6.13	−1.20	7.0	7.94
$Ba_2InDyTe_5$	12.96	−13.47	10.18	10.63
$Ba_2InErTe_5$	11.87	1.44	9.74	9.59

multiplets.[59] The distinct magnetic behavior of $Ba_2InSmTe_5$ is typical for Sm^{3+} chalcogenides.[1,19,20,30]

SHG Measurement. With the use of the 2090 nm laser as the fundamental wavelength, the SHG properties of the noncentrosymmetric Ba_2MLnTe_5 (M = Ga and Ln = Dy, Er, Y; M = In and Ln = Ce, Nd, Sm, Gd, Dy, Er, Y) compounds were measured. Unfortunately, no obvious SHG signals were detected for all of the compounds.

As discussed in the above diffuse-reflectance spectrum measurement and shown in the Electronic Structure Calculation section, the band gaps of the five Ga-containing compounds are around 1.1 eV (1127 nm) and those for the seven In-containing compounds are around 1.3 eV (954 nm). Thus, all 12 compounds have strong absorption of frequency-doubled light (1045 nm) produced through NLO interaction. Moreover, as shown in Figures 5 and 6, all 12 compounds also exhibit strong absorption of the fundamental light of 2090 nm. Thus, failure to detect the SHG signal for the noncentrosymmetric compounds may be due to the strong absorption of both fundamental and frequency-doubled light. In order to experimentally observe the SHG signals of these tellurides, it is necessary to set up a test system using a fundamental light source with a much longer wavelength, such as the CO_2 laser.

Electronic Structure Calculation. In the earlier study on the corresponding selenides in this system, only Ba_2InYSe_5 exhibit strong NLO response, while those containing other rare-earth metals do not. However, no calculation on the electronic structure of Ba_2InYSe_5 was performed. In this work, we calculated the electronic structures of two Y-containing tellurides Ba_2MYTe_5 (M = Ga, In) to better understand their properties. The calculated band structures of Ba_2GaYTe_5 and Ba_2InYTe_5 are plotted along the high symmetry lines in Figures 8 and 9. It is shown that both compounds are direct-gap semiconductors with very similar band structures. The calculated band gaps are 0.922 eV for Ba_2GaYTe_5 and 1.364 eV for Ba_2InYTe_5, which are in good agreement with the values obtained from the diffuse-reflectance spectra. Further calculations with other kinds of pseudopotentials show that the change of the results is not apparent.

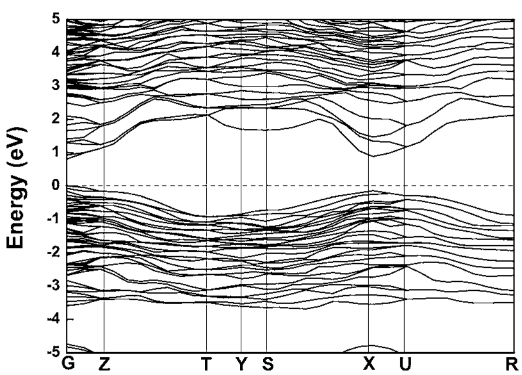

Figure 8. Band structure of Ba_2GaYTe_5.

Figure 10 gives the partial density of states (PDOS) projected on the constitutional atoms in Ba_2GaYTe_5, in which several electronic characteristics can be seen: (i) The Ba 6s and 5p orbitals are strongly localized in the very deep region of the valence band (VB) at about −27 and −16 eV, and so they have no chemical bonding with other atoms. A similar situation exists for Ga 3d orbitals at about −16 eV. (ii) The VB from −10 to −5 eV is mainly composed of the Te 5s orbitals, which have some contribution to the Ga−Te bonding. The upper part of the valence states from −5 eV show some of hybridization between Ba 5d, Te 5p and Ga 4s, 4p orbitals, indicating some chemical bonds between the Ba−Te and Ga−Te atoms. Obviously, the top of the VB maximum is dominated by Te 5p orbitals. (iii) The bottom of the conduction band (CB) is mainly composed of 5p orbitals of Te atoms, although 4d orbitals of Y and 4s orbitals of Ga have some contribution to the electronic level border of CB. The above characteristics indicate that the $^{\infty}_{1}[GaYTe_5]^{4-}$ anionic chain directly determines the energy band gap of Ba_2GaYTe_5.

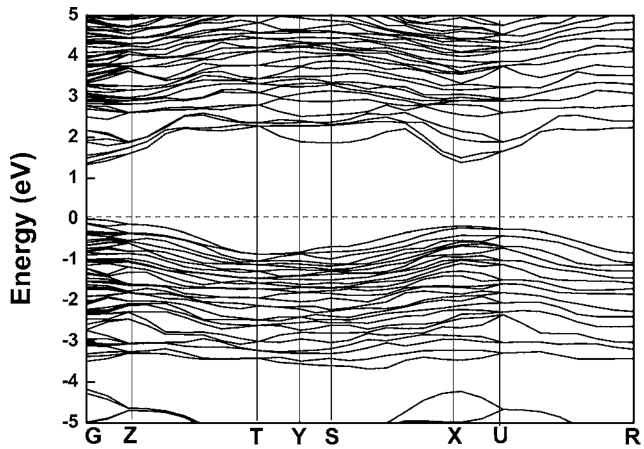

Figure 9. Band structure of Ba_2InYTe_5.

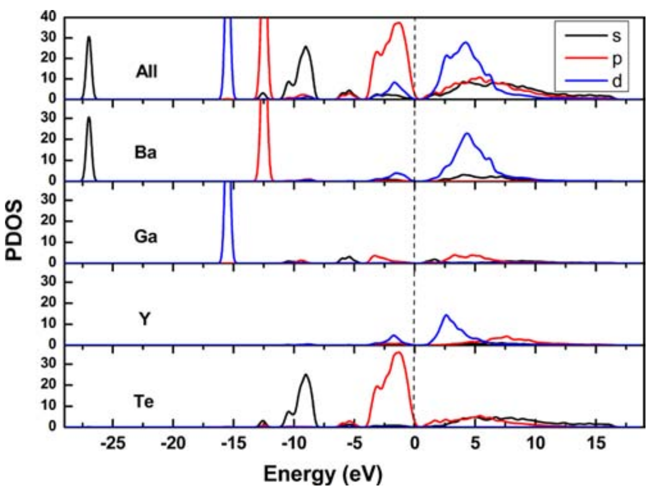

Figure 10. PDOS of Ba_2GaYTe_5.

As shown in Figure 11, the electronic characteristics in the band structure of Ba_2InYTe_5 are very similar to those of Ba_2GaYTe_5, and the $^{\infty}_{1}[InYTe_5]^{4-}$ anionic chains directly determine the energy band gap. As shown in Figures 10 and 11, the Ga 4s and In 5s orbitals have some contribution to the bottom of the CB and the energy of Ga 4s orbitals are lower than In 5s orbitals, which may explain why Ba_2GaYTe_5 possesses a smaller band gap than Ba_2InYTe_5.

On the basis of the above electronic band structures, the virtual excitation processes under the influence of incident radiation were simulated, and the refractive indices and NLO coefficients were obtained. It is well-known that the band gap calculated by LDA is usually smaller than the experimental data because of the discontinuity of exchange-correlation energy. In

dx.doi.org/10.1021/ic301655e | Inorg. Chem. 2012, 51, 11736−11744

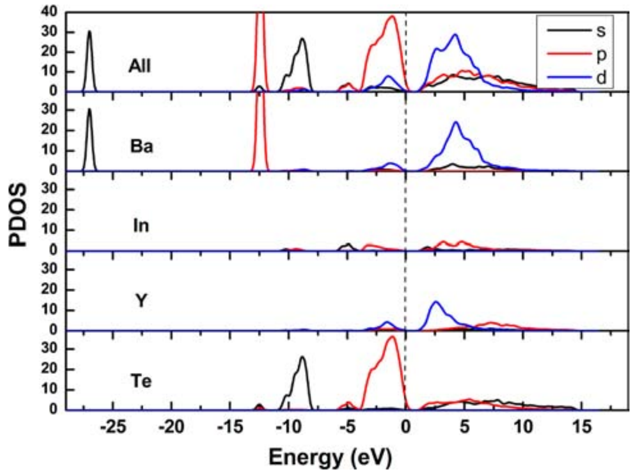

Figure 11. PDOS of Ba_2InYTe_5.

this work, energy scissor operators[60,61] (0.16 eV for Ba_2GaYTe_5 and 0.004 eV for Ba_2InYTe_5) are adopted to shift all of the CBs in order to agree with the measured values of the band gap, which are in a good determination of the low-energy structures in the imaginary part of the dielectric functions. The SHG coefficients of the two crystals were theoretically determined and are shown in Table 7. As discussed earlier, owing to the strong absorption of both the fundamental light (2090 nm) and the frequency-doubled light (1045 nm), we were unable to observe experimentally obvious SHG responses in our test system. However, the large calculated NLO coefficients of these tellurides indicate that they may have NLO application in the far-IR range. Additional experiments, such as NLO characterization with longer wavelength as fundamental light and on bulk single crystals instead of polycrystalline samples, may be necessary to thoroughly evaluate their potential in IR NLO experiments. The calculated NLO coefficients are comparable to those of the traditional $AgGaTe_2$ compound,[56] but $AgGaTe_2$ suffered from a low laser-damage threshold owing, in part, to the defects caused by the disorder between the four-coordinated Ag^+ and Ga^{3+} atoms (vacancies or interstitial ions will be produced to achieve charge balance). Disorder among cations are, however, less likely to happen in Ba_2MYTe_5 (M = Ga, In) because of the different coordination preferences of the cations, which may help to increase the laser-damage threshold. Thus, Ba_2MYTe_5 (M = Ga, In) may be worth further study in view of the NLO properties.

Table 7. Calculated SHG Coefficients of Ba_2MYTe_5 (M = Ga, In)

	Ba_2GaYTe_5	Ba_2InYTe_5
d_{15} (pm/V)	−107.1	−56.4
d_{24} (pm/V)	41.0	14.1
d_{33} (pm/V)	7.7	0.3

■ CONCLUSIONS

In summary, Ba_2MLnTe_5 (M = Ga and Ln = Sm, Gd, Dy, Er, Y; M = In and Ln = Ce, Nd, Sm, Gd, Dy, Er, Y) represent the first tellurides in the quaternary A/M/Ln/Q (A = alkaline earth; M = group IIIA metal Ga, In; Ln = rare earth; Q = S, Se, Te) system. They belong to two different structure types: $Ba_2GaLnTe_5$ (Ln = Sm, Gd) crystallize in the Ba_2GaYSe_5 structure type (space group $P\bar{1}$), while the other 10 compounds Ba_2MLnTe_5 (M = Ga and Ln = Dy, Er, Y; M = In and Ln = Ce, Nd, Sm, Gd, Dy, Er, Y) adopt the Ba_2InBiS_5 structure type in the noncentrosymmetric space group $Cmc2_1$. Both structure types contain $^{\infty}_{1}[MLnTe_5]^{4-}$ chains built from $LnTe_6$ octahedra and MTe_4 (M = Ga, In) tetrahedra, but the $GaTe_4$ tetrahedra are isolated and located on both sides of the chain of $LnTe_6$ octahedra for the first structure type, while for the second structure type, the MTe_4 (M = Ga, In) tetrahedra form a set of chains, which are further connected to only one side of the chain of $LnTe_6$ octahedra. The band gaps of Ba_2MLnTe_5 (M = Ga and Ln = Sm, Gd, Dy, Er, Y; M = In and Ln = Ce, Nd, Sm, Gd, Dy, Er, Y), as deduced from their diffuse-reflectance spectra, are around 1.1−1.3 eV. According to the measurement of diffuse-reflectance spectra, all of the compounds have strong absorption in the entire measured wavelength range from 300 to 2150 nm, so failure to detect the SHG signal in the SHG measurements may be due to the strong absorption of both fundamental light (2090 nm) and frequency-doubled light (1045 nm). According to magnetic susceptibility measurements, the Ba_2MLnTe_5 (M = Ga and Ln = Gd, Dy; M = In and Ln = Gd, Dy, Er) compounds are paramagnetic, obey the Curie−Weiss law, and have effective magnetic moments close to the theoretical values, while $Ba_2InSmSe_5$ does not obey the Curie−Weiss law owing to the crystal-field splitting. Furthermore, on the basis of the electronic structures of Ba_2MYTe_5 (M = Ga, In), their direct band gaps are mainly determined by the $^{\infty}_{1}[MYTe_5]^{4-}$ chains. The calculated NLO coefficients of Ba_2MYTe_5 (M = Ga, In) are comparable to the traditional $AgGaTe_2$ compound. Moreover, the absence of disorder among cations may be beneficial to obtaining high-quality crystals and, hence, increasing the laser-damage threshold.

■ ASSOCIATED CONTENT

Supporting Information

Powder X-ray diffraction patterns of $Ba_2InLnTe_5$ (Ln = Ce, Nd, Sm, Gd, Dy, Er, Y), selected interatomic distances (Å) of Ba−Te for Ba_2MLnTe_5 (M = Ga and Ln = Sm, Gd, Dy, Er, Y; M = In and Ln = Ce, Nd, Sm, Gd, Dy, Er, Y), and crystallographic file in CIF format for Ba_2MLnTe_5 (M = Ga and Ln = Sm, Gd, Dy, Er, Y; M = In and Ln = Ce, Nd, Sm, Gd, Dy, Er, Y). This material is available free of charge via the Internet at http://pubs.acs.org.

■ AUTHOR INFORMATION

Corresponding Author

*E-mail: jyao@mail.ipc.ac.cn.

Notes

The authors declare no competing financial interest.

■ ACKNOWLEDGMENTS

This research was supported by the National Natural Science Foundation of China (Grants 91122034 and 21271178) and the Ministry of Science and Technology of China (973 Project 2011CBA00110).

■ REFERENCES

(1) Liu, Y.; Chen, L.; Wu, L.-M. *Inorg. Chem.* **2008**, *47*, 855−862.
(2) Bucher, C. K.; Hwu, S.-J. *Inorg. Chem.* **1994**, *33*, 5831−5835.
(3) Patschke, R.; Brazis, P.; Kannewurf, C. R.; Kanatzidis, M. G. *Inorg. Chem.* **1998**, *37*, 6562−6563.

(4) Evenson, C. R., IV; Dorhout, P. K. *Inorg. Chem.* **2001**, *40*, 2409–2414.
(5) Zeng, H.-Y.; Mattausch, H.; Simon, A.; Zheng, F.-K.; Dong, Z.-C.; Guo, G.-C.; Huang, J.-S. *Inorg. Chem.* **2006**, *45*, 7943–7946.
(6) Patschke, R.; Heising, J.; Kanatzidis, M. G. *Chem. Mater.* **1998**, *10*, 695–697.
(7) Zhao, H.-J.; Li, L.-H.; Wu, L.-M.; Chen, L. *Chem. Mater.* **2009**, *48*, 11518–11524.
(8) Jin, G. B.; Choi, E. S.; Guertin, R. P.; Booth, C. H.; Albrecht-Schmitt, T. E. *Chem. Mater.* **2011**, *23*, 1306–1314.
(9) Guo, S.-P.; Guo, G.-C.; Wang, M.-S.; Zou, J.-P.; Xu, G.; Wang, G.-J.; Long, X.-F.; Huang, J.-S. *Inorg. Chem.* **2009**, *48*, 7059–7065.
(10) Chen, M.-C.; Li, P.; Zhou, L.-J.; Li, L.-H.; Chen, L. *Inorg. Chem.* **2011**, *50*, 12402–12404.
(11) Zhao, H.-J.; Zhang, Y.-F.; Chen, L. *J. Am. Chem. Soc.* **2012**, *134*, 1993–1995.
(12) Chen, M.-C.; Li, L.-H.; Chen, Y.-B.; Chen, L. *J. Am. Chem. Soc.* **2011**, *133*, 4617–4624.
(13) Huang, F. Q.; Ibers, J. A. *Inorg. Chem.* **1999**, *38*, 5978–5983.
(14) Aitken, J. A.; Larson, P.; Mahanti, S. D.; Kanatzidis, M. G. *Chem. Mater.* **2001**, *13*, 4714–4721.
(15) Zhao, H.-J.; Li, L.-H.; Wu, L.-M.; Chen, L. *Inorg. Chem.* **2010**, *49*, 5811–5817.
(16) Carpenter, J. D.; Hwu, S.-J. *Inorg. Chem.* **1995**, *34*, 4647–4651.
(17) Carpenter, J. D.; Hwu, S.-J. *Chem. Mater.* **1992**, *4*, 1368–1372.
(18) Choudhury, A.; Dorhout, P. K. *Inorg. Chem.* **2008**, *47*, 3603–3609.
(19) Mitchell, K.; Huang, F. Q.; McFarland, A. D.; Haynes, C. L.; Somers, R. C.; Van Duyne, R. P.; Ibers, J. A. *Inorg. Chem.* **2003**, *42*, 4109–4116.
(20) Mitchell, K.; Haynes, C. L.; McFarland, A. D.; Van Duyne, R. P.; Ibers, J. A. *Inorg. Chem.* **2002**, *41*, 1199–1204.
(21) Yao, J.; Deng, B.; Sherry, L. J.; McFarland, A. D.; Ellis, D. E.; Van Duyne, R. P.; Ibers, J. A. *Inorg. Chem.* **2004**, *43*, 7735–7740.
(22) Mitchell, K.; Huang, F. Q.; Caspi, E. N.; McFarland, A. D.; Haynes, C. L.; Somers, R. C.; Jorgensen, J. D.; Van Duyne, R. P.; Ibers, J. A. *Inorg. Chem.* **2004**, *43*, 1082–1089.
(23) Chan, G. H.; Sherry, L. J.; Van Duyne, R. P.; Ibers, J. A. *Z. Anorg. Allg. Chem.* **2007**, *633*, 1343–1348.
(24) Meng, C.-Y.; Chen, H.; Wang, P.; Chen, L. *Chem. Mater.* **2011**, *23*, 4910–4919.
(25) Sutorik, A. C.; Albritton-Thomas, J.; Kannewurf, C. R.; Kanatzidis, M. G. *J. Am. Chem. Soc.* **1994**, *116*, 7706–7713.
(26) Sutorik, A. C.; Albritton-Thomas, J.; Hogan, T.; Kannewurf, C. R.; Kanatzidis, M. G. *Chem. Mater.* **1996**, *8*, 751–761.
(27) Chan, G. H.; Lee, C.; Dai, D.; Whangbo, M.-H.; Ibers, J. A. *Inorg. Chem.* **2008**, *47*, 1687–1692.
(28) Wakeshima, M.; Furuuchi, F.; Hinatsu, Y. *J. Phys.: Condens. Matter* **2004**, *16*, 5503–5518.
(29) Huang, F. Q.; Mitchell, K.; Ibers, J. A. *Inorg. Chem.* **2001**, *40*, 5123–5126.
(30) Yin, W.; Feng, K.; Wang, W.; Shi, Y.; Hao, W.; Yao, J.; Wu, Y. *Inorg. Chem.* **2012**, *51*, 6860–6867.
(31) Pell, M. A.; Ibers, J. A. *Chem. Mater.* **1996**, *8*, 1386–1390.
(32) Malliakas, C.; Billinge, S. J. L.; Kim, H. J.; Kanatzidis, M. G. *J. Am. Chem. Soc.* **2005**, *127*, 6510–6511.
(33) Chemla, D. S.; Kupecek, P. J.; Robertson, D. S.; Smith, R. C. *Opt. Commun.* **1971**, *3*, 29–31.
(34) Boyd, G. D.; McFee, J. H.; Storz, F. G.; Kasper, H. M. *IEEE J. Quantum Electron.* **1972**, *QE-8*, 900–908.
(35) Ohmer, M. C.; Goldstein, J. T.; Zelmon, D. E.; Saxler, A. W.; Hegde, S. M.; Wolf, J. D.; Schunemann, P. G.; Pollak, T. M. *J. Appl. Phys.* **1999**, *86*, 94–99.
(36) Schunemann, P. G.; Setzler, S. D.; Pollak, T. M.; Ohmer, M. C.; Goldstein, J. T.; Zelmon, D. E. *J. Cryst. Growth* **2000**, *211*, 242–246.
(37) *CrystalClear*; Rigaku Corp.: Tokyo, Japan, 2008.
(38) Sheldrick, G. M. *Acta Crystallogr., Sect. A* **2008**, *64*, 112–122.
(39) Gelato, L. M.; Parthé, E. *J. Appl. Crystallogr.* **1987**, *20*, 139–143.
(40) Kurtz, S. K.; Perry, T. T. *J. Appl. Phys.* **1968**, *39*, 3798–3813.
(41) Payne, M. C.; Teter, M. P.; Allan, D. C.; Arias, T. A.; Joannopoulos, J. D. *Rev. Mod. Phys.* **1992**, *64*, 1045–1097.
(42) Clark, S. J.; Segall, M. D.; Pickard, C. J.; Hasnip, P. J.; Probert, M. I. J.; Refson, K.; Payne, M. C. *Z. Kristallogr.* **2005**, *220*, 567–570.
(43) Rappe, A. M.; Rabe, K. M.; Kaxiras, E.; Joannopoulos, J. D. *Phys. Rev. B* **1990**, *41*, 1227–1230.
(44) Lin, J. S.; Qteish, A.; Payne, M. C.; Heine, V. *Phys. Rev. B* **1993**, *47*, 4174–4180.
(45) Kleinman, L.; Bylander, D. M. *Phys. Rev. Lett.* **1982**, *48*, 1425–1428.
(46) Monkhorst, H. J.; Pack, J. D. *Phys. Rev. B* **1976**, *13*, 5188–5192.
(47) Geng, L.; Cheng, W.-D.; Lin, C.-S.; Zhang, W.-L.; Zhang, H.; He, Z.-Z. *Inorg. Chem.* **2011**, *50*, 5679–5686.
(48) Narducci, A. A.; Yang, Y.-T.; Digman, M. A.; Sipes, A. B.; Ibers, J. A. *J. Alloys Compd.* **2000**, *303*, 432–439.
(49) Bentien, A.; Budnyk, S.; Prots, Yu.; Grin, Yu.; Steglich, F. *J. Alloys Compd.* **2007**, *442*, 345–347.
(50) Deiseroth, H. J.; Mueller, H. D. *Z. Anorg. Allg. Chem.* **1996**, *622*, 405–410.
(51) Shannon, R. D. *Acta Crystallogr.* **1976**, *A32*, 751–767.
(52) Feng, K.; Yin, W.; Yao, J.; Wu, Y. *J. Solid State Chem.* **2011**, *184*, 3353–3356.
(53) Bera, T. K.; Jang, J. I.; Ketterson, J. B.; Kanatzidis, M. G. *J. Am. Chem. Soc.* **2009**, *131*, 75–77.
(54) Schevciw, O.; White, W. B. *Mater. Res. Bull.* **1983**, *18*, 1059–1068.
(55) Eifler, A.; Riede, V.; Brückner, J.; Weise, S.; Krämer, V.; Lippold, G.; Schmitz, W.; Bente, K.; Grill, W. *Jpn. J. Appl. Phys.* **2000**, *39*, 279–281.
(56) Isaenko, L.; Krinitsin, P.; Vedenyapin, V.; Yelisseyev, A.; Merkulov, A.; Zondy, J.-J.; Petrov, V. *Cryst. Growth Des.* **2005**, *5*, 1325–1329.
(57) O'Connor, C. J. *Prog. Inorg. Chem.* **1982**, *29*, 203–283.
(58) Kittel, C. *Introduction to Solid State Physics*, 6th ed.; Wiley: New York, 1986.
(59) Kahn, O. *Molecular Magnetism*; VCH Publishers: New York, 1993.
(60) Godby, R. W.; Schluter, M.; Sham, L. *J. Phys. Rev. B* **1988**, *37*, 10159–10175.
(61) Wang, C. S.; Klein, B. M. *Phys. Rev. B* **1981**, *24*, 3417–3429.